Marine Geology 437 (2021) 106505

Contents lists available at ScienceDirect

Marine Geology

journal homepage: www.elsevier.com/locate/margo

The Guadiaro-Baños contourite drifts (SW Mediterranean). A geotechnical approach to stability analysis

M. Yenes [a,*], D. Casas [b], J. Nespereira [a], N. López-González [c], D. Casalbore [d], S. Monterrubio [a], B. Alonso [b], G. Ercilla [b], C. Juan [b,e], P. Bárcenas [c], D. Palomino [c], P. Mata [f], P. Martínez-Díaz [g], N. Pérez [g], J.T. Vázquez [c], F. Estrada [b], M. Azpiroz-Zabala [h], M. Teixeira [i]

[a] Departamento de Geología, Universidad de Salamanca, 37008 Salamanca, Spain
[b] Departament Geociències, Institut de Ciències del Mar, ICM-CSIC, Passeig Marítim de la Barceloneta 31-49, 08003 Barcelona, Spain
[c] Instituto Español de Oceanografía, Centro Oceanográfico de Málaga, Puerto Pesquero s/n, 29640, Fuengirola, Málaga, Spain
[d] Dipartimento Scienze della Terra, Università Sapienza di Roma, Piazzale Aldo Moro 5, 00185 Rome, Italy
[e] Université de Lille, CNRS, Univ. Littoral Côte d'Opale, UMR 8187 - LOG - Laboratoire d'Océanologie et de Géosciences, F-59000 Lille, France
[f] Instituto Geológico y Minero de España (Spanish Geological and Mining Institute), 23 Ríos Rosas, 28003 Madrid, Spain
[g] Igeotest, Ausiàs March, 17600 Figueres, Girona, Spain
[h] Delft University of Technology, Civil Engineering and Geosciences, Stevinweg 1, 2628 CN Delft, the Netherlands
[i] Instituto Dom Luíz, Faculdade de Ciências da Universidade de Lisboa, Edifício C1, Campo Grande, 1749-016 Lisbon, Portugal

ARTICLE INFO

Editor: Michele Rebesco

Keywords:
Contourite drift
Submarine landslide
Alboran Sea
Sedimentology
In-situ geotechnical tests (CPTu)
Factor of safety (FoS)

ABSTRACT

Two Quaternary plastered contourite drifts, with terraced and low-mounded morphologies, make up the continental slope and base-of-slope in the northwestern Alboran Sea, respectively, between the Guadiaro and Baños turbidite systems, close to the Strait of Gibraltar.

Considering their significant lateral extent, the link between the contourite drift deposits and landslides may be particularly important for hazard assessment. The physical properties, composition and geometry of contourite drifts have been proposed as key factors in slope stability, although this relationship still needs to be better constrained. In this work, new *in-situ* geotechnical data (cone penetration tests; CPTu) has been combined with morphostratigraphic, sedimentological, and (laboratory) geotechnical properties to determine the stability of the Guadiaro-Baños drifts.

For the depositional domains of both drifts, the resulting sedimentary and geotechnical model describes low-plasticity granular and silty sands on the erosive terraced domain that evolve seawards to silty and silty-clay deposits with a higher plasticity and uniform geomechanical properties. For the shallower coarse-grained contourite sediments, the cohesion (c') and internal friction angle (ϕ') values are 0–9 kPa and 46–30°, respectively, whereas for the distal fine contourites the undrained shear strength gradient (∇S_u) is 2 kPa/m. These properties allow us to establish high factors of safety for all the scenarios considered, including seismic loading. Slope failure may be triggered in the unlikely event that there is seismic acceleration of PGA > 0.19, although no potential glide planes have been observed within the first 20 m below the seafloor.

This suggests that the contourite drifts studied tend to resist failure better than others with similar sedimentary characteristics. The interplay of several processes is proposed to explain the enhanced undrained shear strength: 1) the geometry of the drifts, defined by an upper contouritic terrace and lower low-mounded shapes; 2) recurrent low-intensity earthquakes with insufficient energy to trigger landslides, favouring increased strength due to dynamic compaction; and 3) cyclic loading induced by solitons/internal waves acting on the sediment.

* Corresponding author.
E-mail addresses: myo@usal.es (M. Yenes), davidcasas@icm.csic.es (D. Casas), jnj@usal.es (J. Nespereira), nieves.lopez@ieo.es (N. López-González), daniele.casalbore@uniroma1.it (D. Casalbore), seramp@usal.es (S. Monterrubio), belen@icm.csic.es (B. Alonso), gemma@icm.csic.es (G. Ercilla), cjuan@icm.csic.es (C. Juan), patricia.barcenas@ieo.es (P. Bárcenas), desiree.palomino@ieo.es (D. Palomino), p.mata@igme.es (P. Mata), patriciam@igeotest.com (P. Martínez-Díaz), normape69@gmail.com (N. Pérez), juantomas.vazquez@ieo.es (J.T. Vázquez), festrada@icm.csic.es (F. Estrada), emeazeta@gmail.com (M. Azpiroz-Zabala), mane.teixeira@gmail.com (M. Teixeira).

https://doi.org/10.1016/j.margeo.2021.106505
Received 2 December 2020; Received in revised form 7 May 2021; Accepted 8 May 2021
Available online 11 May 2021

1. Introduction

Contourite drifts are ubiquitous sedimentary systems, usually with a significant lateral extent and commonly associated with landslides (Laberg and Camerlenghi, 2008; Stow and Faugères, 2008). Sedimentary instability linked to contouritic depositional systems has been observed along many continental margins (Bryn et al., 2005; Rebesco et al., 2014; Krastel et al., 2014; Laberg et al., 2016; Martorelli et al., 2016; Brackenridge et al., 2020; Gatter et al., 2020). Erosive processes associated with bottom currents may, in fact, undermine slopes and cause instability, but contourite sediments may also be prone to failure because of their composition or geometry (Laberg and Camerlenghi, 2008). The development of excess pore pressure, due to high sedimentation rates of fine-grained material or a high organic carbon content, has traditionally been speculated to be an important genetic characteristic closely linked to their destabilisation. Weak layers may also play an important role, as these are where deformation may be initiated, and along which the slip plane would form (*e.g.*, Laberg et al., 2016;

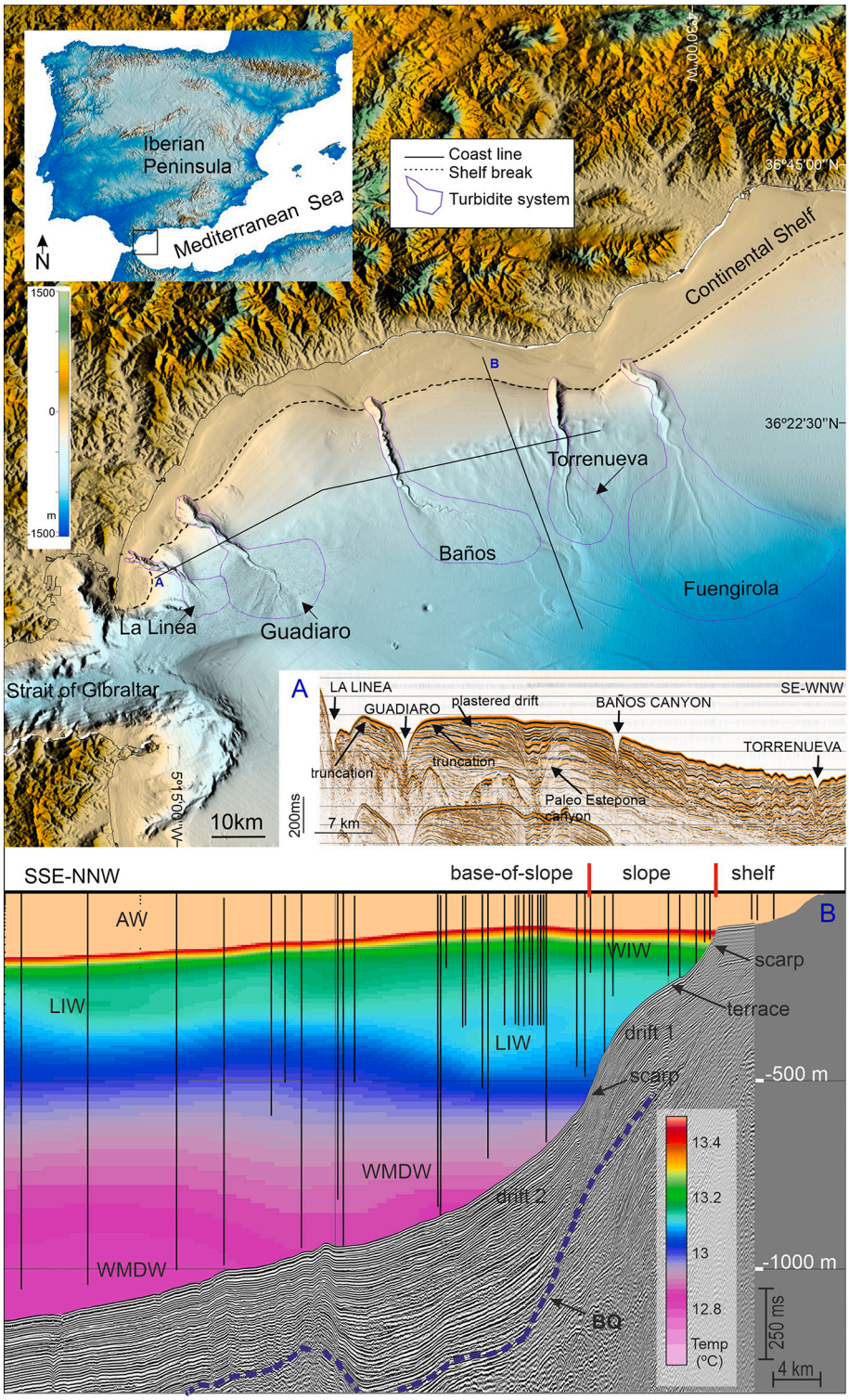

Fig. 1. Multibeam bathymetric map displaying the Spanish margin of the Western Alboran Basin (WAB). Merged bathymetric data from Ercilla et al. (2016), Fauces and Viatar projects. (A) Airgun profile from the ICM-CSIC seismic database (http://gma.icm.csic.es/ca/dades) showings the regional strata pattern interrupted by turbidite systems. (B) Seismic–hydrographic intersections correlating the temperature contrast between water masses (AW, WIW + LIW, and WMDW), the main physiographic domains and sedimentary systems in the area. The black vertical lines in the water column represent CTD stations and the maximum water depth reached for each one. Water-masses were identified using Ocean Data View (ODV) software (http://odv.awi.de). Atlantic Water (AW); Light Mediterranean Waters (LMW) formed by Western Intermediate Water (WIW) and Levantine Intermediate Water (LIW); Western Mediterranean Deep Water (WMDW); Base of Quaternary (BQ).

Miramontes et al., 2018). Whether these landslide-preconditioning factors are a widespread characteristic of contourite drifts still needs to be determined.

Bottom currents play an important role along all the Iberian continental margins, from the Mediterranean to Cantabrian Sea (Stow et al., 2002; Ercilla et al., 2011; Palomino et al., 2011; Hernández-Molina et al., 2011; Casas et al., 2015; Teixeira et al., 2019; Ercilla et al., 2019a; Juan et al., 2020). Sedimentary instability affecting the Cadiz contourite depositional system and Sines Drift, produced by the Mediterranean outflow water (MOW), is evidenced as slide scars and multiple slumps (Lee and Baraza, 1999; Hernández-Molina et al., 2003; Mulder et al., 2003; Alonso et al., 2016; García et al., 2016; Teixeira et al., 2019; García et al., 2020; Mestdagh et al., 2020). Mass wasting associated with drift deposits is observed to the SW of Mallorca (Lüdmann et al., 2012), and particularly on the Palomares margin where the contourites are highly affected by mass transport deposits, ranging from hundreds of meters to a few kilometres in scale (Casas et al., 2019; Ercilla et al., 2019b). In the Alboran Sea, where contourites are ubiquitous, local landslides have only been mapped in the eastern areas and on the seamounts; in contrast, in the western Alboran Sea, landslides seem to be practically absent (Casas et al., 2011; Ercilla et al., 2011, 2016; Alonso et al., 2014).

The aim of this work is to contribute to the understanding of the physical characteristics that explain why contourites may, or may not, be prone to failure. The study focuses on contourites located on the western Spanish margin of the Alboran Sea, between the Guadiaro and Baños turbidite systems (Figs. 1 and 2), where no major sedimentary instabilities have been observed. The study uses conventional sediment cores, as well as acoustic, geophysical and *in-situ* measurements, to characterise the physical and geotechnical aspects of the contourite deposits. *In-situ* cone penetration tests (CPTu) of contourite features are scarce, but are essential for determining the conditions leading to excess pore pressure or the presence of weaker layers.

2. Geological and oceanographic framework

The Alboran Sea is situated in the south-westernmost Mediterranean and is characterised by a complex physiography controlled by Miocene structural changes (Alonso and Maldonado, 1992; Maldonado et al., 1992; Duggen et al., 2004; Ballesteros et al., 2008; Martínez-García et al., 2017; Estrada et al., 2018). The Alboran Basin developed in a convergent tectonic setting during the Upper Oligocene-Miocene rifting

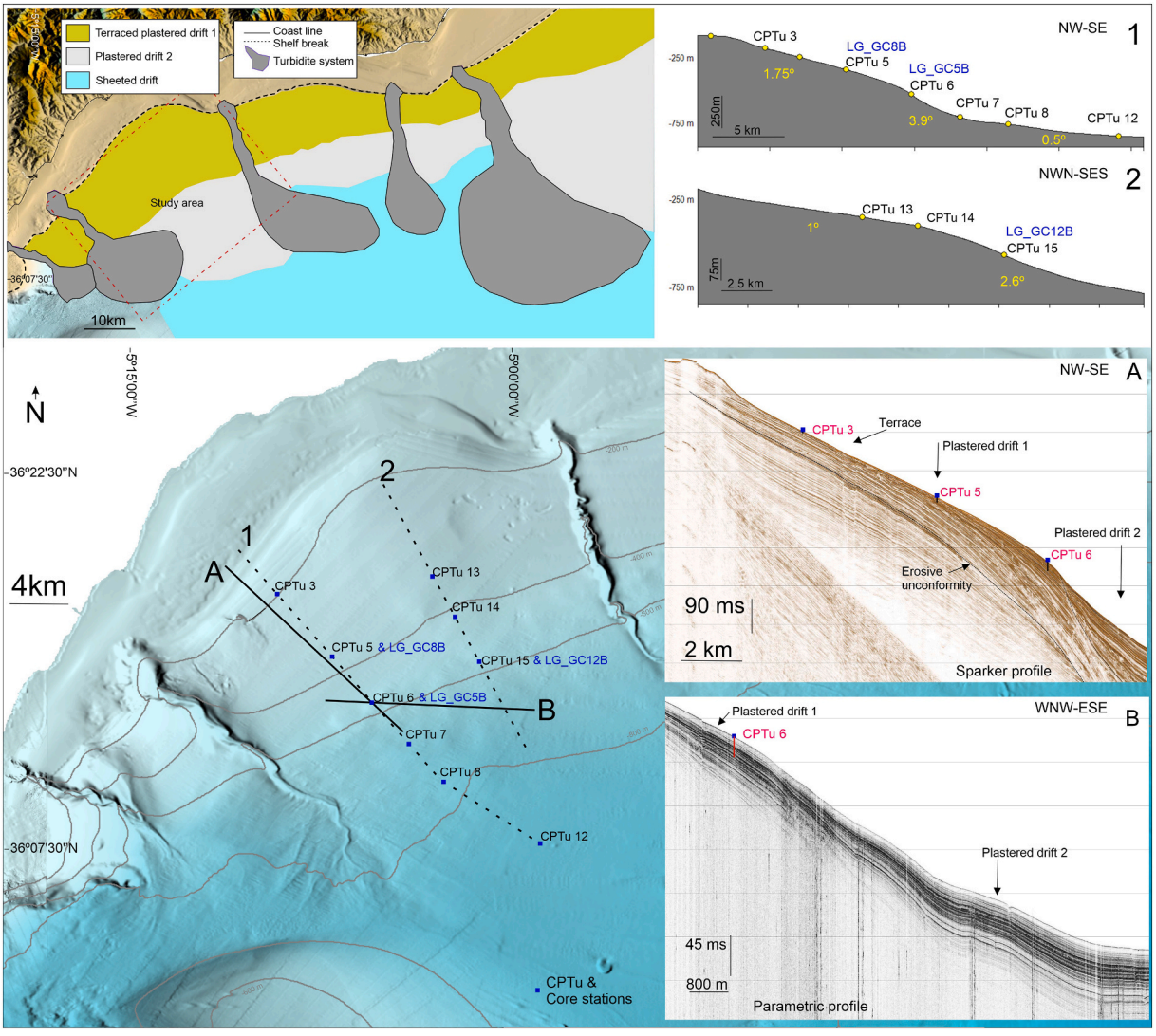

Fig. 2. Map of the lateral distribution of the contourite drifts studied, based on Ercilla et al., 2016. The bathymetric profiles (1 and 2) show the slope gradient of different domains and the position of the gravity cores (LG_GC) and CPTu tests in the study area. Sparker (A) and Topas seismic profiles (B) show the general stratigraphic architecture and eco-facies of the contourites studied. Depths of *in-situ* tests have also been correlated (and projected) with the seismic profiles. Two-way travel distance in miliseconds within the sediments measured on the profiles has been converted to meters using an average velocity of 1600 m/s.

between the Eurasian and African plates (Platt and Vissers, 1989; Comas et al., 1992; Dillon et al., 1980; Dewey et al., 1989). The Alboran Basin dried out during the Messinian Salinity Crisis and after the opening of the Strait of Gibraltar (5.46 to 5.33 Ma) a mega-flood caused prominent excavation and erosion, defining one of the most important changes in the history of both the Mediterranean as a whole and the Western Alboran Basin (WAB) in particular, generating terraces and escarpments (Estrada et al., 2011; Juan et al., 2020). After this episode, the sedimentation began to be influenced by the Mediterranean waters flowing towards the Strait of Gibraltar (Juan et al., 2016).

The physiography of the Spanish margin of the Alboran Sea is defined by a shelf break located at approximately 90–115 m water depth (mwd), an irregular continental slope that extends down to 575–945 mwd, and a base-of-slope down to 600–945 mwd (Ercilla et al., 2016). The sedimentation is mostly siliciclastic, generated primarily by coastal erosion and the rivers that erode the Betic mountains (>3000 m high) bordering the Spanish margin (Lobo et al., 2014; López-González et al., 2019). From morphological and sedimentary perspectives, the margin is dominated by turbidite systems (La Linea, Guadiaro, Baños, Torrenueva, Fuengirola; Fig. 1) and contourite deposits (Ercilla et al., 2019a). Different water masses define the water column: i) the surficial Atlantic Water (AW), that enters the Mediterranean Sea through the Strait of Gibraltar moving towards the N at up to 100 cm/s and extending down to 150–250 mwd; ii) the Light Mediterranean Waters (LMW), comprising the Western Intermediate Water (WIW) and Levantine Intermediate Water (LIW). This extends down to 500–600 mwd, and its near-bottom layers preferentially affect the Spanish slope, moving towards the Strait of Gibraltar at velocities of up to 14 cm/s; iii) and the Western Mediterranean Deep Water (WMDW), below 500–600 mwd, which can move in pulses of up to 22 cm/s. Its near-bottom layer primarily affects the Moroccan margin and deep basins (Gascard and Richez, 1985; Fabrés et al., 2002; Ercilla et al., 2016).

The long-term action of bottom-current processes during the Plio-Quaternary have shaped and deeply influenced the sedimentary evolution of all the physiographic provinces (Ercilla et al., 2016). Recent stratigraphic, geomorphological, and morphological analyses have recognised the ubiquity of both depositional and erosive contourite features (Ercilla et al., 2016; Juan et al., 2016; Fig. 1). Two large plastered drifts (drift 1 and 2; Figs. 1 and 2), associated with the influence of the LMW and the WMDW, characterise the Spanish continental slope and base-of-slope (Ercilla et al., 2016).

3. Dataset and methods

This work is based on the study of combined acoustic (bathymetric), geophysical (seismic reflection), sedimentological (sediment core), and geotechnical (sediment core and CPTu) data obtained in the framework of the FAUCES project, on one cruise aboard the B/O Sarmiento de Gamboa in 2018 (Fig. 2; Table 1).

Several multibeam echosounder datasets, obtained using Kongsberg-Simrad EM-120 and ATLAS Hydrosweep DS sounders (14.5 to 16 kHz) were merged to produce a digital topography model (DTM) with a cell size of 20 m, as shown in Fig. 2. Parametric profiles (very high-resolution TOPAS profiles) with <150 m penetration were used simultaneously with high-resolution, sparker profiles (Fig. 2). TOPAS employs primary (15–21 kHz) and secondary frequencies of 0.5–6 kHz, whilethe Geo-Spark (sparker) sources generate a high-resolution frequency spectrum of between 150 and 3000 Hz. Seismic records showed in Fig. 1 were obtained with airgun systems (140 to 530 c.i.) and are included in the database from the ICM-CSIC (http://gma.icm.csic.es/ca/dades).

Table 1
Gravity cores (LG_GC) and *in-situ* geotechnical tests (CPTu); mwd: meters water depth.

Sample	Latitude (N)	Longitude (W)	mwd (m)	Length (m)
LG_GC-8B	36.253852	−5.121042	336	0.73
LG_GC-12B	36.245266	−5.022043	563	3.05
LG_GC-5B	36.170682	−5.049448	761	3.16
CPTu 3	36.293861	−5.158361	174	4.75
CPTu 5	36.253900	−5.120921	343	11.16
CPTu 6	36.220396	−5.092043	534	19.80
CPTu 7	36.195453	−5.070381	700	18.91
CPTu 8	36.171209	−5.049390	756	19.81
CPTu 12	36.098991	−5.048783	835	19.79
CPTu 13	36.303286	−5.055120	346	19.79
CPTu 14	36.280708	−5.041488	396	19.63
CPTu 15	36.245205	−5.021796	564	19.42

The sedimentary characteristics of the gravity cores recovered (Table 1) were determined from a textural analysis performed using a Coulter LS 100 laser particle size analyser (Fig. 3). Mineral phases in the clay levels were also identified through X-ray diffraction using a BRUKER D-8 Advance with Cu Kα radiation, working at a scan rate of 2 ɵ/min. Oriented aggregates were also prepared to identify the clay fraction. The physical properties (density) of the cored sediments were measured over whole core sections, at 1 cm intervals, using a Geotek Multisensor Core Logger (MSCL) (Fig. 4). The geotechnical properties (AENOR, 1999) were analysed in selected sections of the gravity cores (Table 2; Fig. 4); these included water content, void ratio, bulk density, grain size analyses, and Atterberg limits. The results allowed us to classify the samples according to the Unified Soil Classification System (USCS) (ASTM D2487, 2011). To study sediment compressibility, seven one-dimensional consolidation tests were run using a conventional oedometer to estimate the compression index (Cc or sediment compressibility), the recompression index (Cs, or Cc during reloading stages), and the overconsolidation ratio (OCR) resulting from σ'_p/σ'_{v0}, where σ'_p is the maximum previous effective overburden pressure (preconsolidation pressure), and σ'_{v0} is the *in-situ* vertical effective stress (current overburden pressure assuming hydrostatic conditions). In addition, the oedometric modulus (E_m) and permeability coefficient (k) were determined in each test (AENOR, 1999).

Nine sites were tested using a DATEM Neptune 5000 penetrometer following 2 transects crossing the contourite drifts (1 and 2 in Fig. 2). This CPTu is able to recover data up to 20 m below the sea floor. It has a thrust capacity of 35 kN, push rod diameter of 19 mm, and was equipped with a 5 cm^2 cone penetrometer. During the tests, a 20 mm/s penetration rate was applied, with a vertical resolution of 2 cm. Tip resistance (q_t), sleeve friction (f_s), and pore water pressure (u, position u_2) were measured during the tests. Before starting the test, the sea bottom pore pressure was measured ($u_{seabottom}$). This reference value was selected as the "zero value" during the test and, consequently, $u = (u_{measured} - u_{seabottom})$. At the CPTu sites located at water depths beyond the range of the cone used (> 500 m), the f_s was either not, or only partially, recorded. Problems have been reported when working in deep water (Lunne, 2012), as all the sensors register a large force at the seabed due to the hydrostatic pressure.

Using the specific software gINT and the Datgel CPT tool, the parameters measured during the test allowed us to obtain various derived parameters.

For many CPTu correlations, the *in-situ* total unit weight (γ_t) is required to assess the total overburden stress (σ_{vo}). The following empirical equation, developed by Mayne (2010) and used in Steiner et al. (2015), was introduced into the calculations:

$$\gamma_t = 11.46 + 0.33 \cdot \log(z) + 3.10 \cdot \log(f_s) + 0.70 \cdot \log(q_t)$$ where (z) is the penetration depth.

Even though this expression sometimes underestimates the γ_t at the seafloor (up to 2.5 m depth), the agreement is much better for deeper sediments (Steiner et al., 2015). In CPTu performed in water depths beyond the range of the cone used, an *in-situ* total unit weight (γ_t) of 17 kN/m^3 was assigned for the depth range 0–10 m, and 18 kN/m^3 for 10–20 m. These values were chosen considering the trend of MSCL density log.

The sediments tested in each CPTu were classified according to Robertson Soil Behaviour Types (SBT classification; Robertson, 1990).

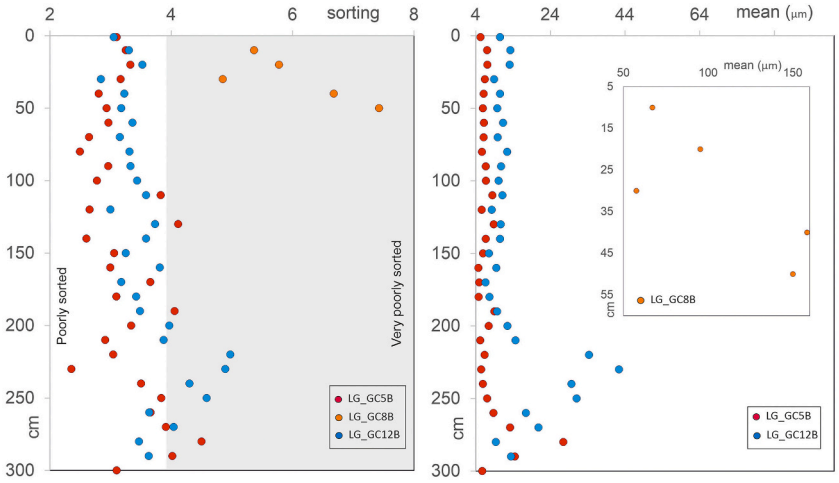

Fig. 3. Mean grain size (right) and sediment sorting (left) of cores sampled.

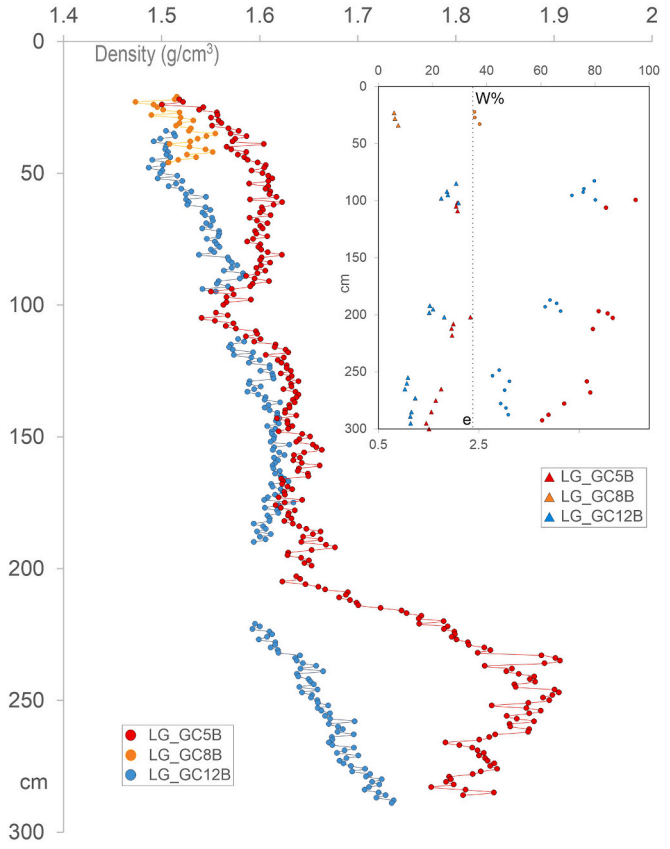

Fig. 4. Physical and geotechnical properties of cores LG_GC5B, LG_GC8B, and LG_GC12B. The solid lines on the left represent the density calculated from the MSCL results. On the right: void ratio (e) and water content (w %) obtained through laboratory tests on selected samples.

This is basically a function of f_s and q_t or B_q, which is the pore pressure ratio defined by the expression:

$$B_q = \frac{u - u_o}{q_t - \sigma_{vo}}$$

where (u) is the pore pressure measured, (u_o) is the hydrostatic pore pressure and (σ_{vo}) is the vertical overburden total stress at the corresponding depth.

For the strength, a generally accepted equation was applied to determine the *in-situ* undrained shear strength (S_u) for clayey soils:

$$S_u = \frac{q_t - \sigma_{vo}}{N_{kt}}$$

where N_{kt} is the empirical correlation factor, which typically ranges from 10 to 18 (a value of 14 was adopted). The shear strength of the coarse-grained sediments was assessed according to the expression in Campanella et al. (1983) for the effective internal friction angle (ϕ') using cone penetration resistance (q_t) and the *in-situ* vertical effective stress (σ'_{vo}):

$$tan(\phi') = \frac{1}{2.68}\left[log\left(\frac{q_t}{\sigma'_{vo}}\right) + 0.29\right]$$

The *in-situ* vertical effective stress (σ'_{vo}) was calculated considering the vertical overburden pressure (σ_{vo}) according to the *in-situ* total unit weight (γ_t) and assuming hydrostatic conditions for the pore pressure ($u_o = z_w \gamma_w$, where z_w is the depth from the sea bottom).

In addition to *in-situ* tests, various geotechnical analyses were performed on selected samples to study sediment strength. The undrained shear strength (S_u) was obtained from unconsolidated undrained (UU) triaxial tests performed using a GDS Triaxial Testing System (GDSTTS) with a 38/50-mm Bishop and Wesley cell. The effective cohesion (c') and effective friction angle (ϕ') were obtained from the consolidated

Table 2
Results of geotechnical tests on selected samples.

CORE	Depth (cm b.s.f.)	Grain size (%)			Atterberg limits (%)		USCS
		Sand	Silt	Clay	LL	PI	
LG_GC8B	27	59	25	16	28.1	4.1	SM
	67	70	17	13	NP	NP	SM
LG_GC12B	4	1	51	48			
	47	2	53	45			
	105	1	53	46	57.5	22.7	MH
	147	2	47	51	57.6	23.1	MH
	205	4	52	44	52.3	21.9	MH
	247	19	54	27	31.9	8.8	ML
	295				44.5	17.3	ML
	297	4	53	43			
LG_GC5B	5	1	38	61	71.3	34.1	MH
	105	2	37	61	66.5	31.9	MH
	204	2	36	62	65.8	27.5	MH
	313	3	46	51	53.5	25.1	CH

cm b.s.f.: centimeters below sea floor. LL, Liquid Limit; PI, Plasticity Index; USCS, Unified Soil Classification System (SM: silty sand; MH: high-plasticity silt; ML: low-plasticity silt; CH: high-plasticity clay).

undrained (CU) triaxial test and consolidated drained (CD) shear strength tests using a conventional direct shear box.

Slope stability analyses were carried out using the 2-D limit equilibrium slope stability software Slide 8.0, Rocscience Inc. The Generalised Limit Equilibrium method (GLE) analyses the forces (or stresses) that act on a failure surface. To determine the Factor of Safety (FoS: ratio between the resisting shear strength and the sum of all mobilised shear stresses) the Bishop simplified method (Bishop, 1955) was selected. A slope stability analysis for drained and undrained conditions, including seismic activity, was designed to assess the sediment instability dynamics over time. The stability of the slope under seismic load was evaluated according to a pseudostatic analysis (*e.g.*, Leynaud et al., 2004). To implement this analysis using the GLE method, the models must include both the horizontal and vertical static loads to simulate the inertia generated by the earthquake acceleration; this method assumes that the pseudostatic forces generated by an earthquake (F_h: horizontal; F_v: vertical) remain constant over long periods of time. The pseudostatic force value used in the analysis is one-half of the peak ground acceleration (PGA) calculated for the study area (Yenes et al., 2019).

4. Results and interpretations

4.1. Morphology and stratigraphy

The study area comprises 610 km^2 where two Quaternary plastered contourite drifts make up the continental slope and base-of-slope, just as they do in the rest of the northwestern Alboran Sea, influenced by both the LMW and the WMDW (Ercilla et al., 2016; Ercilla et al., 2019a; Juan et al., 2020; Fig. 1). An eastward-prograding contourite drift has developed between 190 and 600 mwd. This drift is characterised by its terraced morphology. Seaward, another low-mounded plastered contouritic drift has developed on the base-of-slope beyond 600 mwd (Fig. 2). Erosive features can be observed in the proximal domains of both plastered drifts (*i.e.*, the terrace and the surface/scarp defining the transition to the lower plastered drift), whereas the distal domains present depositional characteristics (Ercilla et al., 2019a). The upper continental slope morphology is determined by the smooth relief of the contourite terrace (1–1.75°); this gradient increases seaward as it transitions to the lower plastered drift, where it reaches 3.9° (Fig. 2). The base-of-slope presents very low relief, with an average gradient of 0.5° (Fig. 2).

Contourite drifts represent important accumulations of sediments, up to 315 ms in thickness (twtt). Drift facies are defined by layered deposits with internal erosive unconformities, while the terrace and scarp present continuous subparallel stratified facies and truncated reflections (Fig. 2).

4.2. Sedimentological properties

The cored sediments sampled from the plastered drifts have a mean grain size of between 4 and 160 μm and are poorly and very poorly sorted (Fig. 3). On the contourite terrace (LG_GC8B) of the plastered drift, the sediments are basically sands (>60%) with low quantities (<15%) of clays. Seawards they are mostly muddy but have abundant sandy layers; the presence of these decreases in the plastered base-of-slope deposits, where the sediments are more than 95% silty-clays (Table 2). X-ray diffraction analysis revealed that the muddy sediments comprise more than 50% clay minerals, among which illite is the most abundant, accounting for up to 27% (Table 3).

The SBT classification (from the CPTu) allows us to deduce a longer sedimentary column (almost 20 mbsf, meters below sea floor) due to the deep penetration of the CPTu tests (Table 1). Only at the shallowest sites (CPTu3 at 174 mwd, and CPTu5 at 343 mwd) was there low penetration, associated with the predominance of sand and gravelly sand (Fig. 5). At CPTu13 (346 mwd) and CPTu14 (396 mwd) there was greater penetration, where sands were crossed in the first 10 m, with silty-clays and clays down to 20 m. This trend changed in CPTu6, 7, 8, 12 and 15 (*i.e.*, towards deeper areas) where the sedimentary column is dominated by silty-clay to clay sediments (Fig. 5).

Table 3
X-ray diffraction results for samples retrieved from LG_CG-5B at 203 and 313 cm below sea floor.

	LG_GC5B-203 (%)	LG_GC5B-313 (%)
kaolinite	10	11
quartz	27	28
smectite	7	4
illite	27	26
calcite	18	16
chlorite	8	10
dolomite	1	2
K feldspar	–	1
plagioclase	2	2

4.3. Physical and index properties

The results of both the discrete and continuous physical and index property analyses of the cores are summarised in Table 2 and Fig. 4. Atterberg limits testing was conducted on several selected samples from cores LG_GC5B, LG_GC8B, and LG_GC12B. The results indicated an average liquid limit of 53 and a plasticity index of 21.6, with the lowest values (*i.e.*, very low plasticity) corresponding to the shallowest core, LG_GC8B. Most of the samples were therefore classified as MH or ML soils (*i.e.*, silts of high-low plasticity), except for the sandy LG_GC8B samples that were classified as SM (silty sand).

Continuous density measurements yielded average values of 1.52 to 1.67 g/cm^3 for all the cores, with silty-clay sediments having the highest densities (up to 1.9 g/cm^3). The downcore density trends in LG_GC5B and LG_GC12B were similar, and we were able to observe the effects of low-level progressive consolidation due to overburdening. In LG_GC5B, from 2 to 2.7 m, there was a local increase in density due to the presence of a silty-clayey level, however from 2.70 the trend became similar in the two cores (Fig. 4). The measurements of decreasing void ratios and pore water with depth, presenting typical values for cohesive sediments, were consistent with this interpretation (Table 2). All the parameters recorded for LG_GC12B indicated a relative increase in the silty-clay character towards the distal or deepest part of the drift. In contrast, the record for LG_GC8B was limited, with considerable scatter due to its sandy character (*e.g.*, $e < 1$).

4.4. Consolidation and compressibility

The oedometer tests showed that the sediment of the contourite drifts was normally consolidated to slightly overconsolidated, with an OCR ranging from 0.90 to 3.50 (Table 4). Higher OCR values (>1), found within the upper 1 mbsf, could be explained by apparent overconsolidation (AOC), which is common in surface sediments. AOC is related to the formation of a structured sediment generated by both secondary consolidation and ageing processes (Yenes et al., 2020).

The compression and recompression index (Cc and Cs) and the oedometric modulus (E_m) showed that the coarser sediments from the slope plastered drift terrace were less compressible (LG_GC8B: Cc = 0.1719, E_m = 28,261 kPa) than the finer sediments located in the distal domain and in the base-of-slope plastered drift (average for LG_GC12B and LG_GC5B: Cc = 0.5241, E_m = 12,212 kPa).

The permeability coefficient for the contourites ranged between 1.36×10^{-9} m/s (high values at the surface) and 8.26×10^{-10} m/s, with an average of 1.09×10^{-9} m/s; these are common values for contourite deposits (*e.g.*, Miramontes et al., 2018). In general, the permeability was greatest in the terrace and the first few centimeters of the cores, and decreased towards the deepest areas.

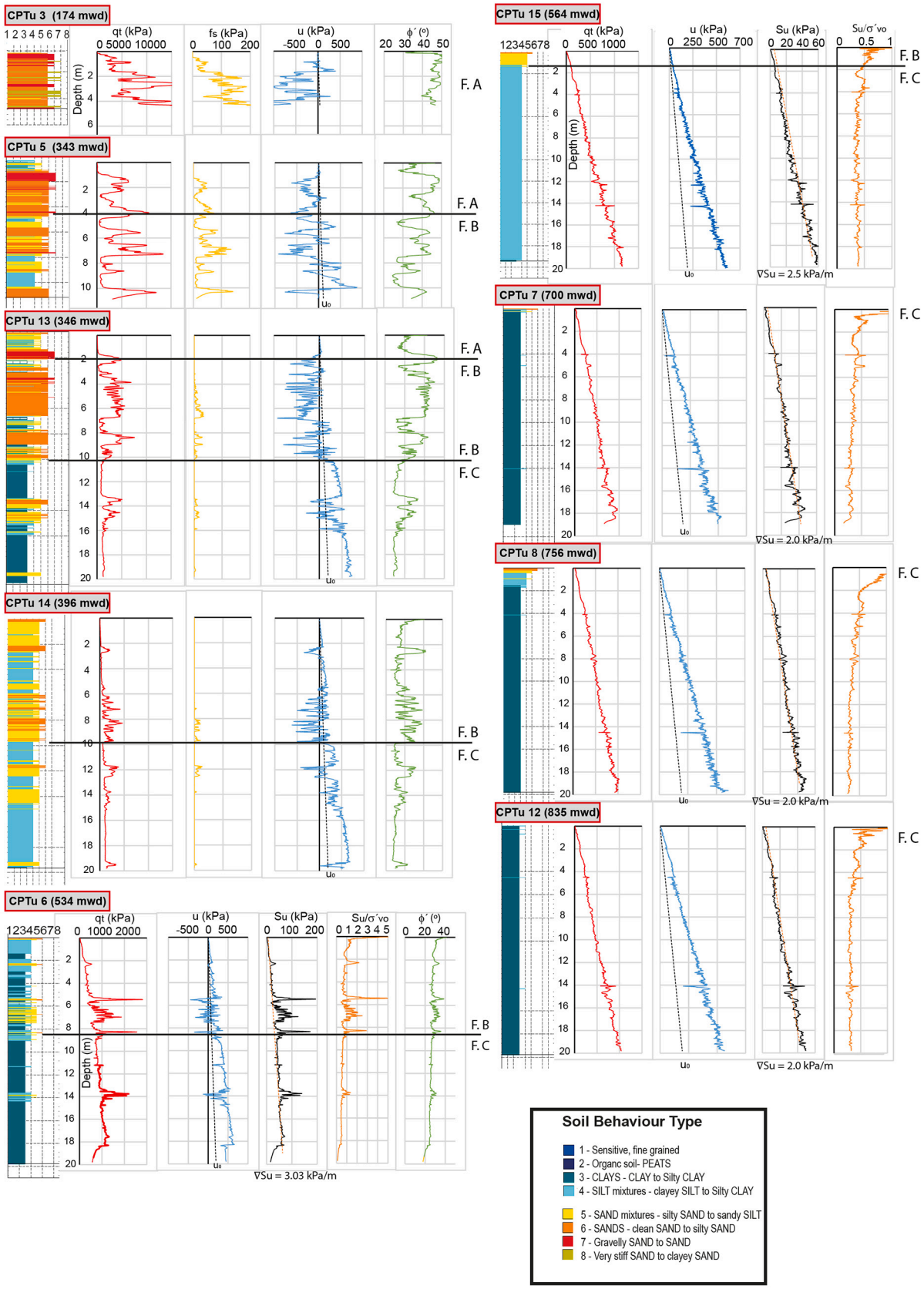

Fig. 5. Processed and corrected CPTu data: (q_t) corrected cone resistance; (f_s) sleeve friction; (u) pore pressure, black dotted lines indicate hydrostatic pressure (u_0); (ϕ) effective friction angle; (S_u) undrained shear strength, brown dotted lines indicate general trend; (S_u/σ'_{vo}) ratio between undrained shear strength and *in-situ* effective pressure. SBT according to Robertson (1990). Geotechnical facies: Facies A (F.A), Facies B (F.B), Facies C (F.C). The locations of the CPTu sites are shown in Fig. 2. The abrupt changes in the parameters at 14 mbsf that are observed in CPTu 7, 8, 12 and 15 are not significant, since they correspond to interruptions in the penetration rate for dissipation tests. (For interpretation of the references to colour in this figure legend, the reader is referred to the web version of this article).

Table 4
Results of the oedometer tests.

CORE	Depth (cm b. s.f.)	Cc	Cs	E_m (kPa)	OCR	k (m/s)
LG_GC8B	32	0.1719	0.0131	28,261	3.50	1.41×10^{-9}
LG_GC12B	102	0.5308	0.0819	12,120	1.70	1.36×10^{-9}
	202	0.4872	0.0730	12,110	1.12	8.26×10^{-10}
	303	0.3432	0.0614	14,964	0.90	6.37×10^{-10}
LG_GC5B	98	0.6511	0.1120	10,761	1.88	2.03×10^{-9}
	202	0.6766	0.1280	10,622	1.06	5.52×10^{-10}
	313	0.4557	0.0986	12,697	0.98	5.32×10^{-10}

Cc, compression index; Cs, recompression index; Em, oedometric modulus (measured for a load between 929.7 and 1910.7 kPa); OCR, overconsolidation ratio; k, permeability coefficient.

4.5. Strength properties

The strength parameters were determined from the results of laboratory tests performed on selected samples (Table 5). These parameters obtained in the laboratory are useful for analysing the slope stability as well as verifying the *in-situ* CPTu test results. In the only core where a vertical series was tested (LG_GC12B), the undrained shear strengths (S_u) from the laboratory triaxial tests (UU) showed a clear trend, increasing with depth. The values ranged from 4.2 kPa at 2.55 mbsf to 16.9 kPa at 2.6 mbsf; additionally, the S_u for LG_CG-5B was lower than for LG_GC12B at a similar depth below the seafloor (Table 5).

The effective cohesion (c') and effective friction angle (ϕ') for drained conditions were obtained through direct shear tests (CD) and the consolidated undrained triaxial test (CU). The results indicated that the sediments from the contourite terrace (LG_GC8B) present typical values for sandy sediments (ϕ' = 35.9°), while towards the deeper areas (LG_GC12B and LG_GC5B) the internal friction angle is less (mean values between 28.7° and 24.8°), due to the prevalence of silty-clay to clay sediments.

Table 5
Results from the shear strength (CD: consolidated drained test) and triaxial tests (UU: unconsolidated undrained test; CU: consolidated undrained test).

CORE	Depth (cm b.s.f.)	TEST	Strength Parameters		
			S_u (kPa)	c' (kPa)	ϕ' (°)
LG_GC8B	28	Direct Shear (CD)	–	9.0	35.9
LG_GC12B	85	Triaxial UU	5.0	–	
	95	Direct Shear (CD)	–	5.3	27.3
	195	Direct Shear (CD)	–	3.8	28.2
	255	Triaxial UU	8.2	–	
	265	Triaxial UU	16.9	–	
	273	Triaxial CU	–	0	33.4
	292	Direct Shear (CD)	–	7.4	25.9
LG_GC5B	105	Direct Shear (CD)	–	2.7	27.3
	212	Direct Shear (CD)	–	4.7	23.7
	275	Triaxial CU	–	5	22.8
	295	Triaxial UU	4.1	–	
	304	Direct Shear (CD)	–	6.3	25.4

S_u, undrained shear strength; c', effective cohesion; ϕ', effective friction angle.

4.6. Cone penetrometer test (CPTu)

Three geotechnical facies were differentiated based on the SBT classification and mechanical response during the *in-situ* tests (Fig. 5):

Facies A: These correspond to the coarser granular sediments tested in the area, defined in CPTu 3, the top (0–4 mbsf) of CPTu 5, and the top (0–2 mbsf) of CPTu 13. This facies mainly corresponds to types 6 and 7 of the SBT classification. The main types of sediment are coarse sands.

Facies B: These correspond to granular sediments found throughout intervals 4 to 10 mbsf in CPTu 5, 2–10 mbsf in CPTu 13, and the top of sites CPTu 14 (0–10 mbsf), CPTu 6 (0–9 mbsf), and CPTu 15 (0–1.75 mbsf). They mainly correspond to types 5 and 6 of the SBT classification. They are predominantly sands.

Facies C: These correspond to the finest sediments found, defined at the bottom of CPTu 13, 14, 6, and 15, and throughout the entire sedimentary column recorded from CPTu 7, 8, and 12. They mainly correspond to types 3 and 4 of the SBT classification. The main types of sediment are silty clays and clays.

The tip resistance results for granular sediments gave a high q_t (up to 15,000 kPa), whereas finer material tended to give a lower q_t (up to 1000 kPa at 20 mbsf). The granular sediments presented a q_t gradient from the highest values in the shallow contouritic terrace down to 5000 kPa towards the distal domain of the terrace (CPTu 14, 396 mwd); the finer sediments presented a linear increase in q_t with depth. Sleeve friction (f_s) decreased from values of 100 kPa in shallow granular sediments to lower values as the sediment became finer (Fig. 5). In water depths beyond the range of the cone used (> 500 m), the f_s was not, or only partially, recorded.

The pore pressure (u) recorded in granular (high permeability) sediments tended to be in equilibrium with the hydrostatic pressure (u_o), although at some sites there was negative excess pore pressure (Fig. 5); they have been interpreted as dilatant layers, where these sudden decreases in the pore water pressure (u) with values dropping below the reference value ($u_{seabottom}$), resulting $u < 0$ are not unusual. For the low-permeability fine sediments, excess pore water pressures were recorded, of up to 500 kPa at 20 mbsf (Fig. 5).

The geotechnical property (derived from CPTu data) needed to analyse slope stability under undrained conditions is the undrained shear strength (S_u), whereas the friction angle (ϕ') is used for the drained case (Fig. 5). Drained failure is related to slow loading conditions or the granular character of the sediment, such as those defining geotechnical Facies A and B. In these cases the ϕ' varied from 24° to 46°, as seen in geotechnical Facies A. CPTu-based undrained shear strength gradients (∇S_u) gave 2 kPa/m (CPTu 7, 8 and 12), and 3.03 and 2.5 kPa/m for CPTu 6 and 15 (Fig. 5). Furthermore, the ratio between the undrained shear strength and *in-situ* effective pressure (S_u/σ'_{vo}) confirms the overconsolidation of the most superficial sediments (Fig. 5; Dan et al., 2007), which, as already indicated, could be explained by AOC (Yenes et al., 2020).

4.7. Slope stability analysis

A simplified slope model can be constructed by combining the stratigraphic architecture (Fig. 2) of the two large plastered drifts and the geotechnical facies, defined using CPTu and core analyses. The erosive contourite terrace is defined by geotechnical facies A, while the depositional mounded domain of the slope-plastered drift 1 associated with the LMW is defined by geotechnical Facies B. The stratigraphically lower part of this drift (>10 mbsf), as well as the plastered drift 2, associated with the influence of the WMDW, presents homogenous geotechnical properties, defined by Facies C (Fig. 6).

Slope stability has been evaluated for various scenarios: 1) considering the geotechnical properties used for slope stability analysis under undrained conditions, *i.e.*, the undrained shear strength (S_u) and the submerged unit weight (γ'); 2) considering the geotechnical properties under drained conditions, *i.e.*, the submerged unit weight (γ'), the

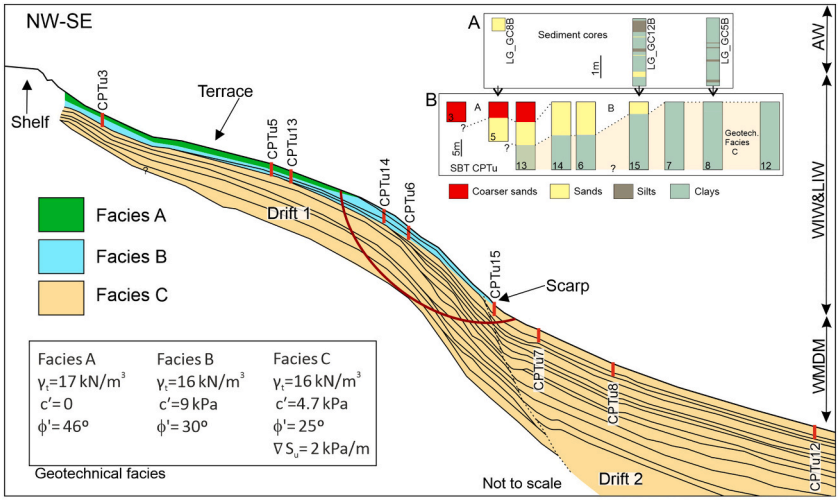

Fig. 6. Geotechnical model superposed onto the stratigraphic architecture of the contourite drifts. Three geotechnical facies (A, B, C) define the mechanical behaviour of the sedimentary deposits forming the two drifts (1 and 2). The model describes a granular erosive contourite terrace that evolves at depth to silty-clayey domains with uniform geomechanical properties. The red line indicates a potential basal failure surface, identified as the most probable for the stability model used. (A) Synthetic sedimentary log of sediment cores and their correspondence with the CPTu sites (arrows). (B) Correlation of SBT results, grouped by main (representative) types of sediment, for the CPTu sites that define the geotechnical facies. See discussion in Section 5.1 for slightly divergences in terms of grain size results (SBT *vs* gravity cores). (For interpretation of the references to colour in this figure legend, the reader is referred to the web version of this article.)

effective cohesion (c'), and the friction angle (ϕ'); and 3) considering that seismic loading develops in undrained conditions (a seismic shock is rapid enough to prevent the excess pore pressure from dissipating, Strasser et al., 2007). The results, using the most common slope gradients in the area (Fig. 2) and the slope gradient needed to reduce the FoS to <1, are summarised in Table 6.

An analysis of slope stability for static conditions reveals that contourite sediments are stable (FoS > > 1) for the typical slope angles found (average 3° up to a maximum in the transition to the lower drift of 5°), and for both drained and undrained conditions. The slope stability assessment shows that even with higher slope gradients than those observed in the area (except for the canyon walls) the sediment is stable (Table 6).

Taking a peak ground acceleration (PGA, a_b/g) of 0.12 (obtained from regional data for a 475-year return period (Gaspar-Escribano et al., 2015), in all locations the sediment remains stable. With a corrected PGA, in order to consider a potential amplification effect over the sediment (Roesner et al., 2019), the value increases up to 0.19 (Table 6).

$$a_c = S \cdot \rho \cdot a_b$$

where (S) is the amplification coefficient and (ρ) is a hazard coefficient which can be 1 or 1.3 (NCSE-02, 2009).

Even with this increased shaking effect the sediment comprising the contourite drift remains stable (Table 6). The model informs us that to reach values of FoS < 1 slope gradients as high as 13° are necessary.

5. Discussion

This work characterises the sedimentological, physical and geotechnical features of contourite deposits using conventional sediment cores in addition to *in-situ* measurements. This allows us to compare the results and analyse any discrepancies between the two approaches, providing useful insights for geotechnically characterising similar deposits in future studies, as discussed in Section 5.1. The overall stability of the contourite deposits in the study area has been determined, suggesting that factors such as morphology may play a role in the slope stability, as discussed in Section 5.2.

Table 6
Factors of Safety (FoS) calculated for the most common slope gradients in the area (average = 3°; maximum in the transition to the lower drift = 5°) and for the theoretical slope gradient needed to reduce the FoS enough to trigger failures. These "extreme" slopes are only present in areas like canyon sidewalls.

Slope angle (°)	Static conditions		Earthquake loading conditions (UC)	
	DC	UC	PGA = 0.12	PGA = 0.19
3–5	7.990	5.817	2.224	1.629
13–22	2.597	1.612	1.038	0.854

(DC) Drained conditions; (UC) Undrained conditions; (PGA) Peak Ground Acceleration.

5.1. Sedimentological and geotechnical properties. In-situ vs laboratory properties

The sedimentological and geotechnical characteristics of the slope and base-of-slope plastered drifts located between the Baños and Guadiaro turbidite systems have been defined using two convergent methods, laboratory tests and *in-situ* measurements, the latter having almost never been applied in this type of sedimentary environment. The resulting geotechnical model describes a sandy/granular erosive contourite terrace that evolves at depth to silty or silty-clayey depositional domains with uniform geomechanical properties (Fig. 6).

Although the sedimentary columns described using sedimentary tests and SBT classification are generally coherent, there are certain discrepancies that may be associated with methodological issues. The SBT classification of CPTu 5 and 8 diverges in terms of grain size results, defining top intervals with finer (silty for CPTu 5) or coarser (sandy for CPTu 8) sediments than are, in fact, present (Figs. 5 and 6). This can be explained by the absence of sleeve friction (f_s) during the test, which reduces the accuracy of the geotechnical stratigraphy. It can also be explained, for the most surficial sediments, by the AOC effect that occurs at the top of marine sedimentary successions (Table 4). Minor divergences in the results from the uppermost stratigraphy of CPTu 6 and 7 are also associated with this AOC (Yenes et al., 2020). Pore pressure (u) helps us to identify the potential artefacts observed in the SBT classification. In the case of CPTu 5, (u) tends to be in equilibrium with the hydrostatic pressure (u_0), coinciding with granular deposits (Fig. 5); here the perturbation of the cone penetration is rapidly dissipated as water can move quickly through this type of sediment. In the case of CPTu 8, the excess pore water pressure recorded is compatible with normally consolidated and fine-grained sediments (Fig. 5); in these low permeability materials, the recovery of the initial theoretical hydrostatic conditions requires a longer period of time.

The comparison of strength parameters (*in-situ vs* tested sediment) reveals some differences. Although the triaxial and direct shear tests (Table 5) are in agreement with the CPTu-based shear strength, defining low values of S_u (< 10 kPa), discrepancies can be seen when the results are compared. The shear strength for LG_GC5B/CPTu 8 is higher when measured using the *in-situ* equipment (for example at 3 mbsf), while for LG_GC12B/CPTu 5, at 2.65 mbsf, the result of the UU test is double the

value obtained with the *in-situ* equipment. S_u is a non-intrinsic parameter, as its value depends on several changing factors, including strain rate, stress history, type of failure, strength anisotropy, and so on (Robertson and Cabal, 2014; Low et al., 2010). Consequently, any discrepancies may be related to the unavoidable disturbance of very soft and soft materials during the preparation and placement of the samples to be tested, modifying the stress history of the sediment. Consequently, the correlation between the S_u from the CPTu and S_u from the laboratory test depends on the empirical parameter N_{kt}, which is a parameter with a significative dispersion.

Fig. 7 compares the friction angle (ϕ) values obtained from both the CPTu tests (ϕ'CPTu) and laboratory tests (DS and TCU) (ϕ'LAB). For each direct shear and triaxial tests 10 cm and 30 cm of sample were used respectively to prepare the specimens to be tested; the ϕ'CPTu considered is, therefore, the average value calculated from the same depth ranges in the corresponding piezocone. There is good agreement between the *in-situ* and laboratory results. Only the result of one triaxial test displays a significant difference between the two methods. The points are distributed on both sides of the fit line, and it cannot therefore be stated that the test type (*in situ* or laboratory) conditions the maximum φ′ value.

5.2. Sediment strength enhancement

Present-day contourites in the WAB show no evidence of large-scale instability features (Fig. 1; Ercilla et al., 2016; Casas et al., 2011). Only a few small-scale features have been described, and these are mostly in the sub-bottom sedimentary record (Fig. 8; Ercilla et al., 1992; Baraza et al., 1992; Casas et al., 2011). This contrasts with the nearby Palomares margin, located to the NE on the Iberian margin (Casas et al., 2019), where the contourites can be correlated with those of the WAB, although in this case the contourite features of the slope have been intensively reworked by instability processes (Ercilla et al., 2019a).

The main triggers for submarine landslides are related to decreased shear strength in the sediments. The sedimentological and geotechnical properties defining the contourite drifts developed between the Guadiaro and Baños turbidite systems explain why the geotechnical model presents high factors of safety. The contourite drifts are predominantly defined by granular (low plasticity; very poorly sorted) terraced slope sediments that evolve at depth to medium- to high-plasticity, low-permeability and normally consolidated-slightly overconsolidated silty clayey-sediments. The muddy (cohesive) sediments are rich in illite and kaolinite (Table 4), which correlates positively with shear resistance (Müller-Vonmoos and Loken, 1989). The AOC in the surface layers, which affects some of the tested areas, may act, locally, as strengthening factor. The empirical model suggests that AOC may increase the FoS up to 61.5% for 5° slopes with a 1 m layer presenting AOC (Yenes et al., 2020).

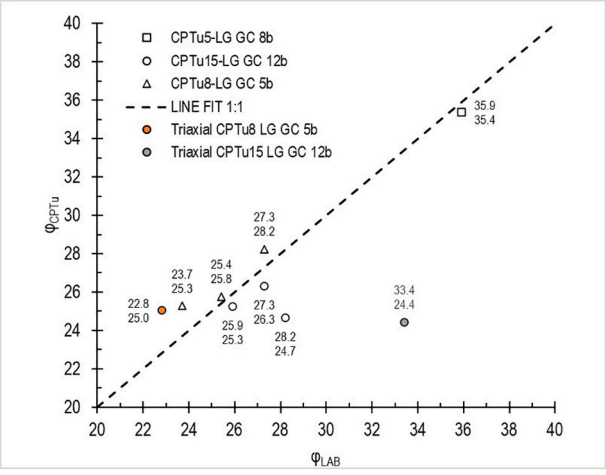

Fig. 7. Effective friction angles obtained from laboratory tests (φ′ LAB) and piezocone test (ϕ' CPTu).

One factor favouring the decreased shear strength is the generation of excess pore pressure. This process can develop due to, among other causes, gas migration and gas-hydrate dissociation. Neither published studies nor our seismic data point to the presence of gas flow or reduced gas-hydrate stability conditions at any depth contributing to this effect in the area between the Guadiaro and Baños turbidite systems (Fig. 2).

In-situ geotechnical tests show that there are no zones of rapid shear strength change in which glide planes could develop, at least within the first 20 mbsf. This is a key issue in this zone and the data can only be improved by increasing the range of the *in-situ* tests to detect deeper weak layers. Although differences may be related to the rate at which the stresses are applied, the plastered drifts studied do tend to resist failure better than others with similar lithologies and physical properties (*e.g.*, Laberg et al., 2016; Miramontes et al., 2018; Casas et al., 2019; Ercilla et al., 2019b).

Here, we propose various processes that could explain the increased stability compared to other continental slope drifts in the Western Mediterranean (*e.g.*, Casas et al., 2019):

5.2.1. Geometry

Plastered drifts are often mounded sediments that form gentle slopes. Although the gradients resulting from contourite deposition are only occasionally greater than the previous slope, drifts may generate local surfaces with slope increases. In the study area, the gentle gradients of the terraced slope-plastered drift, and the low mound morphology of the base-of-slope plastered drift may condition the stability of these sediments and increase the overall strength of the whole system (Puzrin et al., 2015; Miramontes et al., 2018). Conversely, the erosional scarp defining the transition to the plastered drift 2 may have the opposite effect. The slope adjacent to the study area, and linked to the increased gradient of this surface (> 7°), is the only location where minor mass flow deposits have been observed in the western part of this margin (Fig. 8). We used this information to model a new synthetic morphology for the study area. The results show that if the terraced morphology were mounded and the basal erosion were greater, the FoS would decrease by around 28%.

5.2.2. Seismic strengthening

Seismic strengthening is a process by which frequent and low intensity earthquakes that do not have enough energy to trigger landslides strengthen the sediment *via* dynamic compaction (Locat and Lee, 2002; Lee et al., 2007; Strozyk et al., 2010). This process has been postulated to explain the low frequency of submarine landslides in several sei smically active areas (McAdoo et al., 2004; McAdoo and Watts, 2004; Camerlenghi et al., 2010; Strozyk et al., 2010; Strasser et al., 2012; Sawyer and DeVore, 2015; Ikari and Kopf, 2015). This seismic strengthening increases the shear strength, or generates sedimentary intervals with similar compositions but different resistance parameters according to the frequency of earthquakes in different geological periods (Ikari and Kopf, 2015; Yenes et al., 2020).

The Central Alboran Sea is a tectonically active area, there have been significant recent earthquakes (Mw = 6.4; www.ign.es) and it is affected by submarine landslides (Alonso et al., 2014; Casas et al., 2011, 2015; Galindo-Zaldivar et al., 2018). Conversely, for the last two decades in the study area (WAB), more than 200 events have been recorded. The frequency-magnitude distribution is defined by the median value of Mw = 2 and 75% of the earthquakes (Q3) lies below Mw = 2.6 (seismic data from www.ign.es). This low level seismicity in the study area provides evidence for how seismic strengthening has played a role in controlling slope stability.

5.2.3. Oceanographic strengthening

The present-day water depth of the AW/WIW + LIW interface dips

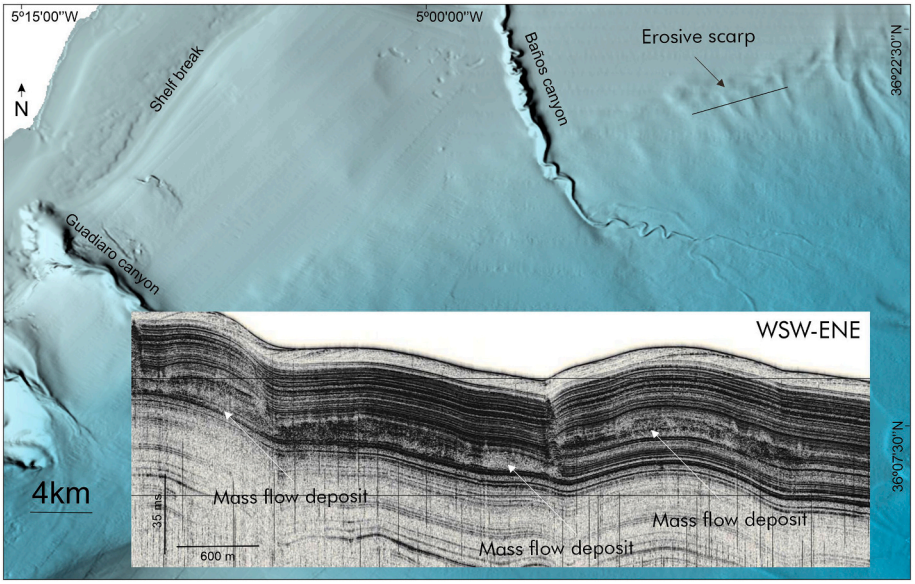

Fig. 8. Small mass-flow deposits on the slope adjacent to the Guadiaro-Baños system, associated with the presence of the erosive scarp that marks the transition to plastered drift 2 occupying the base-of-slope. The Topas profile is taken from the ICM-CSIC seismic database (http://gma.icm.csic.es/ca/dades).

southwards along the Spanish slope. This interface is an intense pycnocline, affected by phenomena such as internal waves (*e.g.*, McCave et al., 2001; Cacchione et al., 2002; Puig et al., 2004). This oceanographic setting could have shifted vertically during the high-frequency and high-amplitude Quaternary sea level changes, thus affecting different intervals of the contouritic terraced seafloor (Ercilla et al., 2016). In addition, large perturbations in the current velocity are induced by internal waves. Solitons have also been observed propagating from the Strait of Gibraltar into the Alboran Sea, as well as above the terraced plastered drift, and reaching bottom depths of 400 m (Armi and Farmer, 1988; Bruno et al., 2002; Vázquez, 2006). Various types of internal waves are generated within the Strait of Gibraltar: one produces variations in the pycnoclines according to the tidal period; others are superimposed, with short periods and large amplitudes (Jacobsen and Thomsen, 1934, in Vázquez, 2006). This phenomenon produces current oscillations of up to 0.4 m/s with wavelengths of up to 1500 m, amplitudes between 15 and 100 m, and periods from 10 to 60 min or cycles of 0.001 Hz (Jacobsen and Thomsen, 1934; Frasseto, 1964; La Violette et al., 1986; Armi and Farmer, 1988; Bruno et al., 2002; Puig et al., 2004; Vázquez, 2006). Wave trains are not continuous and require certain conditions, such as high atmospheric pressure in the Mediterranean area and surficial current speed >1 m/s (Vázquez, 2006).

Because of their cyclic effect, internal waves may strengthen the sediment. de Rouck and van Damme (1996) developed a method for measuring the effect of waves and tides on the seafloor, which involves a time-dependant function to calculate the excess pore water pressures generated by applying the wave compression:

$$u\,(0,t) = u_o cos\left(\frac{2\pi x}{L} - \frac{2\pi t}{T}\right) = u_o cos\left(\frac{2\pi t}{L}\right)$$

where u_o is the pore pressure, depending either

on the tide $(u_o = \gamma_w H_{sea})$

or the wave $\left(u_o = \frac{\gamma_w}{n}\cdot\frac{H}{2cos\left(\frac{2\pi d}{L}\right)}\right)$

and (H_{sea}) is the tidal range, (H) is the wave height, (T) is the wave period, (L) is the wavelength, (d) is the water depth, and (n) is the Grace correction coefficient.

Applying this method adapted to internal waves, and following the first method (depending on the tide), H_{sea} would be $H_{isopynic}$ or the wave amplitude, which is 60 m in the Strait of Gibraltar (Vázquez, 2006), with a density difference between AW/WIW + LIW of 2 kg/m^3:

$$\Delta u_o = \Delta\rho_w \cdot g \cdot H_{isopynic} = 2\ \frac{kg}{m^3}\cdot g \cdot 60\ m = 1176\ \frac{N}{m^2} \sim 1.2\ kPa$$

According to the second method (*i.e.*, depending on the wave) where L = 1500 m and d = 170 m, the result is $\Delta u_o = 0.436\ kPa$.

In both cases, the excess pore water pressures generated tend to be in equilibrium with the hydrostatic pressure at a depth that depends on the permeability and the wave period (Fig. 9). The low excess pore water

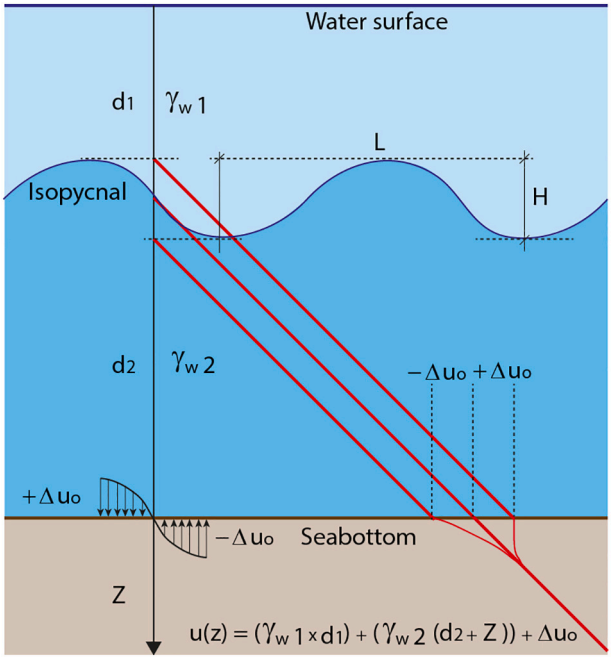

Fig. 9. Diagram of the pore pressure variation at the sea bottom, as a consequence of the passage of internal waves.

pressures calculated (0.4 to 1.2 kPa) are not enough to affect the stability of the deposits, although in a similar way to the seismic dynamic compaction, they may be a strengthening factor (Lee et al., 2007).

The effect of internal waves depends on the geotechnical characteristic of the deposits with which they interact. The internal waves modelled for this area, when affecting geotechnical Facies A, will produce more stable and resistant internal structures. The high permeability and dilatant characteristics observed of this facies (CPTu 3, 5 and 13, Fig. 5) will facilitate this effect. Small cyclical loads will locally increase the effective pressure enough to contribute to the rearrangement of sedimentary particles.

However, if internal waves acted on cohesive sediments (*e.g.*, geotechnical Facies B and C) there are diverse potential effects. Normally consolidated sediments under a cyclic load will suffer increased pore pressure that may or may not dissipate (in function of sediment permeability and the frequency of the waves). If dissipation occurs, the sediment will consolidate, improving its resistance. If the frequency of the waves does not allow the excess pore pressure to dissipate, the sediment may destabilise. In other settings, for example with overconsolidated sediments and long-enough periods of wave train cycles, the excess of pore pressure could also be dissipated (Thian and Lee, 2017).

Internal waves may be considered a strengthening factor for the upper domain of contouritic drift 1, similar to seismic dynamic compaction (Lee et al., 2007; Strozyk et al., 2010). However further observations and more accurate characterisation are needed to better constrain their effects.

6. Conclusions

Large Quaternary plastered drifts (drift 1 and 2), affected by the action of the LMW and WMDW, characterise the slope and base-of-slope in the area between the Guadiaro and Baños turbidite systems. A terraced contourite drift has developed between 190 and 600 mwd, which shows both erosional (in the proximal terrace domain) and depositional features. Seawards, there is another plastered drift influenced by the WMDW, extending from an erosional surface at 600 mwd to beyond the base of slope. The combination of new *in-situ* geotechnical measurements (CPTu) and laboratory testing of the sedimentary and geotechnical features of these contourite drifts enables us to better understand the role contourite processes play in slope stability.

The properties of the contourite drifts enable us to establish a geotechnical model that reveals high factors of safety. The contourite terrace sediments are defined as granular, low plasticity, and very poorly sorted; they evolve at depth to medium- to high-plasticity, low-permeability and poorly sorted silty clayey-sediments, rich in illite and kaolinite, defining the depositional domain of the drifts. The sedimentary results are in agreement with the three geotechnical facies defined using the *in-situ* properties and SBT classification. Together these outline a geotechnical model that merges the two plastered drifts into geotechnical units with uniform geomechanical properties. The *in-situ* tests detected no potential glide planes, at least within the maximum 20 mbsf tested, and this, together with the other properties of the deposits, suggests that these contourite drifts tend to resist failure better than others with similar features. Several characteristics and processes may explain the increased stability, including the geometry of the drift, recurrent low intensity earthquakes, and cyclic loading induced by internal waves.

In the study area, the classical mounded geometry of the plastered drifts has been modified by erosive processes that have resulted in a high degree of stability throughout the entire sedimentary body. The recurrent low-intensity earthquakes registered in the area, which do not have enough energy to trigger failures, may dynamically compact the sediment. A similar effect may be produced by the interaction of the sediments with internal waves.

Our study shows that the rarely gathered *in-situ* CPTu data is critical for better characterising the drifts in a geotechnical sense. Moreover, the geotechnical approach must be seriously considered in order to fully understand the characteristics that condition the stability of contourite drifts.

Data availability

Casas, D., & UTM-CSIC. (2018). *FAUCES-2 Cruise, RV Sarmiento de Gamboa* [Data set]. UTM-CSIC. doi:10.20351/29SG20181004.

Declaration of Competing Interest

The authors declare that they have no known competing financial interests or personal relationships that could have appeared to influence the work reported in this paper.

Acknowledgements

This research was supported by the Spanish Fauces project (CTM2015-65461-C2-1-R). We thank IHS for providing the Kingdom Suite™ licence. This work acknowledges the *'Severo Ochoa Centre of Excellence'* accreditation (CEX2019-000928-S). We are also grateful for the data we received from the Viatar project (http://datos.ieo.es/) and we would like thank to Igeotest for their collaboration. We dedicate this work *in memoriam* to Albert Figueras from the UTM-CSIC in Barcelona.

References

AENOR, 1999. Standard Test Methods for Geotechnical Tests (Soils). Spanish Association of Standardization and Certification, Spain.

Alonso, B., Maldonado, A., 1992. Pliocene–Quaternary margin growth patterns in a complex tectonic setting (Northeastern Alboran Sea). Geo-Mar. Lett. 12 (2/3), 137–143.

Alonso, B., Ercilla, G., García, M., Vázquez, J.-T., Juan, C., Casas, D., Estrada, F., D'Acremont, E., Gorini, C., El Moumni, B., Farran, M., 2014. Quaternary mass-transport deposits on the North-Eastern Alboran Seamounts (SW Mediterranean Sea). In: Krastel, S., Behrmann, J.-H., Völker, D., et al. (Eds.), Submarine Mass Movements and their Consequences, Advances in Natural and Technological Hazards Research, vol. 37, pp. 561–570.

Alonso, B., Ercilla, G., Casas, D., Stow, D.A.V., Rodríguez-Tovar, F.J., Dorador, J., Hernández-Molina, F.J., 2016. Contourite vs gravity-flow deposits of the Pleistocene Faro Drift (Gulf of Cadiz): sedimentological and mineralogical approaches. Mar. Geol. 377, 77–94. https://doi.org/10.1016/j.margeo.2015.12.016.

Armi, L., Farmer, D., 1988. The flow of the Mediterranean water through the Strait of Gibraltar. Prog. Oceanogr. 21, 1–105.

ASTM D2487, 2011. Standard Practice for Classification of Soils for Engineering Purposes (Unified Soil Classification System). ASTM International, West Conshohocken.

Ballesteros, M., Rivera, J., Muñoz, A., Muñoz-Martín, A., Acosta, J., Carbó, A., Uchupi, E., 2008. Alboran Basin, southern Spain—part II: Neogene tectonic implications for the orogenic float model. Mar. Pet. Geol. 25, 75–101. https://doi.org/10.1016/j.marpetgeo.2007.05.004.

Baraza, J., Ercilla, G., Lee, H., 1992. Geotechnical properties and preliminary assessment of sediment stability on the continental-slope of the northwestern Alboran Sea. Geo-Mar. Lett. 12 (2–3), 150–156.

Bishop, A.W., 1955. The use of the slip circle in the stability analysis of slopes. Géotechnique 5, 7–17.

Brackenridge, R.E., Nicholson, U., Sapiie, B., Stow, D., Tappin, D.R., 2020. Indonesian throughflow as a preconditioning mechanism for submarine landslides in the Makassar Strait. In: Georgiopoulou, A., Amy, L.A., Benetti, S., Chaytor, J.D., Clare, M.A., Gamboa, D., Mountjoy, J.J. (Eds.), Subaqueous Mass Movements and their Consequences: Advances in Process Understanding, Monitoring and Hazard Assessments, 500. Geological Society, London, Special Publications, pp. 195–217. https://doi.org/10.1144/SP500-2019-171.

Bruno, M., Alonso, J.J., Cózar, A., Vidal, J., Ruiz-Cañavate, A., Echevaria, F., Ruiz, J., 2002. The boiling-water phenomena at Camarinal Sill, the Strait of Gibraltar. Deep-Sea Res. Part II: Top. Stud. Oceanogr. 49 (19), 4097–4113. https://doi.org/10.1016/S0967-0645(02)00144-3.

Bryn, P., Berg, K., Forsberg, C.F., Solheim, A., Kvalstad, T.J., 2005. Explaining the storegga slide. Mar. Pet. Geol. 22, 11–19.

Cacchione, D., Pratson, L.F., Ogston, A.S., 2002. The shaping of continental slopes by internal tides. Science 296 (5568), 724–727. https://doi.org/10.1126/science.1069803.

Camerlenghi, A., Urgeles, R., Fantoni, L., 2010. A database on submarine landslides of the Mediterranean Sea. In: Mosher, D.C., Shipp, R.C., Moscardelli, L., Chaytor, J.D., Baxter, C.D.P., Lee, H.J., Urgeles, R. (Eds.), Submarine Mass Movements and their

Consequences. Advances in Natural and Technological Hazards Research. Springer, Dordrecht, NL, pp. 503–513.
Campanella, R.G., Robertson, P.K., Gillespie, D., 1983. Cone penetration testing in deltaic soils. Can. Geotech. J. 20, 23–35.
Casas, D., Ercilla, G., Yenes, M., Estrada, F., Alonso, B., García, M., Somoza, L., 2011. The Baraza slide. A sliding model. Mar. Geophys. Res. 32 (1–2), 245–256.
Casas, D., Casalbore, D., Yenes, M., Urgeles, R., 2015. Submarine mass movements around the Iberian Peninsula. The building of continental margins through hazardous processes. Bol. Geol. Min. 126, 257–278.
Casas, D., Ercilla, G., Alonso, B., Yenes, M., Casalbore, D., Nespereira, J., Estrada, F., Chiocci, F., Idárraga-García, J., Teixeira, M., Ceramicola, S., Fauces Cruises Teams, 2019. Submarine mass movements affecting the submarine Almanzora-Alías-Garrucha canyon (SW Mediterranean). In: 34th IAS meeting of sedimentology "Sedimentology to face societal challenges on risk, resources and record of the past". 34 IAS. Meeting of sedimentology, 10-13 September, Rome.
Comas, M.C., García-Dueñas, V., Jurado, M.J., 1992. Neogene tectonic evolution of the Alboran Sea from MCS data. Geomar. Lett. 12, 157–164. https://doi.org/10.1007/BF02084927.
Dan, G., Sultan, N., Savoye, B., 2007. The 1979 nice harbour catastrophe revisited: trigger mechanism inferred from geotechnical measurements and numerical modelling. Mar. Geol. 245, 40–64. https://doi.org/10.1016/j.margeo.2007.06.011.
de Rouck, J., van Damme, L., 1996. Overall slope stability analysis of rubble mound breakwaters. In: 25th International Conference on Coastal Engineering.
Dewey, J.F., Helman, M.L., Turco, E., Hutton, D.H.W., Knott, S.D., 1989. Kinematics of the western Mediterranean. In: Coward, M.P., Dietric, D., Park, R.G. (Eds.), Alpine Tectonics 45. Special Publications, London, UK, Geological Society, pp. 265–283.
Dillon, W.P., Robb, J.M., Greene, H.G., Lucena, J.C., 1980. Evolution of the continental margin of southern Spain and the Alboran Sea. Mar. Geol. 36, 205–226. https://doi.org/10.1016/0025-3227(80)90087-0.
Duggen, S., Hoernle, K., van den Bogaard, P., Harris, C., 2004. Magmatic evolution of the Alboran region: the role of subduction in forming the western Mediterranean and causing the Messinian salinity crisis. Earth Planet. Sci. Lett. 218, 91–108.
Ercilla, G., Alonso, B., Baraza, J., 1992. Sedimentary evolution of the northwestern Alboran Sea during the Quaternary. Geomar. Lett. 12, 144–149. https://doi.org/10.1007/BF02084925.
Ercilla, G., Juan, C., Estrada, F., Casas, D., Alonso, B., García, M., Farran, M., Palomino, D., Vázquez, J.T., Llave, E., Hernández-Molina, J., Medialdea, T., Gorini, C., Gensous, B., Tesson, M., Maldonado, A., Ammar, A., Contouriber and Montera teams, 2011. A new model for the recent sedimentation in the Alboran Sea (SW Mediterranean). In: 28th-IAS Meeting of Sedimentology, Zaragoza, Spain.
Ercilla, G., Juan, C., Hernández-Molina, F.J., Bruno, M., Estrada, F., Alonso, B., Casas, D., Farran, M.L., Llave, E., García, M., Vázquez, J.T., D'Acremont, E., Gorini, C., Palomino, D., Valencia, J., El Moumni, B., Ammar, A., 2016. Significance of bottom currents in deep-sea morphodynamics: an example from the Alboran Sea. Mar. Geol. 378, 157–170. https://doi.org/10.1016/j.margeo.2015.09.007.
Ercilla, G., Juan, C., Periáñez, R., Alonso, B., Abril, J.M., Estrada, F., Casas, D., Vázquez, J.T., d'Acremont, E., Gorini, C., El Moumni, B., Do Couto, D., Valencia, J., 2019a. Influence of along-slope processes on modern turbidite systems and canyons in the Alboran Sea (southwestern Mediterranean). Deep-Sea Res. I 144, 1–16.
Ercilla, G., Galindo-Zaldívar, J., Estrada, F., Valencia, J., Casas, D., Alonso, B., Tendero, V., Comas, M., Sanz de Galdeano, C., Vázquez, J.T., 2019b. New insights in the geomorphology of the Gulf of Vera (western Mediterranean). In: 34th IAS meeting of sedimentology "sedimentology to face societal challenges on risk, resources and record of the past". 34 IAS. Meeting of sedimentology, 10-13 September, Rome.
Estrada, F., Ercilla, G., Gorini, C., Alonso, B., Vázquez, J.T., García-Castellanos, D., Juan, C., Maldonado, A., Ammar, A., Elabbassi, M., 2011. Impact of pulsed Atlantic water inflow into the Alboran Basin at the time of the Zanclean flooding. Geo-Mar. Lett. 31 (5–6), 361–376.
Estrada, F., Galindo-Zaldívar, J., Vázquez, J.T., Ercilla, G., d'Acremont, E., Alonso, B., Gorini, C., 2018. Tectonic indentation in the central Alboran Sea (westernmost Mediterranean). Terra Nova 30, 24–33.
Fabrés, J., Calafat, A., Sánchez-Vidala, A., Canals, M., Heussner, S., 2002. Composition and spatio-temporal variability of particle fluxes in theWestern Alboran Gyre, Mediterranean Sea. J. Mar. Syst. 33–34, 431–456. https://doi.org/10.1016/S0924-7963(02)00070-2.
Frasseto, R., 1964. Short period vertical displacements of the upper layers in the Strait of Gibraltar. In: Technical Report 30. SACLANT ASW Research Centre, La Spezia, Italy, p. 49.
Galindo-Zaldivar, J., Ercilla, G., Estrada, F., Catalán, M., d'Acremont, E., Azzouz, O., 2018. Imaging the growth of recent faults: the case of 2016–2017 seismic sequence sea bottom deformation in the Alboran Sea (western Mediterranean). Tectonics 37, 2513–2530. https://doi.org/10.1029/2017TC004941.
García, M., Hernández-Molina, F.J., Alonso, B., Vázquez, J.T., Ercilla, G., Llave, E., Casas, D., 2016. Erosive sub-circular depressions on the Guadalquivir Bank (Gulf of Cadiz): Interaction between bottom current, mass-wasting and tectonic processes. Mar. Geol. 378, 5–19. https://doi.org/10.1016/j.margeo.2015.10.004.
García, M., Llave, E., Hernández-Molina, F.J., Lobo, F.J., Ercilla, G., Alonso, B., Casas, D., Mena, A., Fernández-Salas, L.M., 2020. The role of late Quaternary tectonic activity and sea-level changes on sedimentary processes interaction in the Gulf of Cadiz upper and middle continental slope (SW Iberia). Mar. Pet. Geol. 121, 104595. https://doi.org/10.1016/j.marpetgeo.2020.104595.
Gascard, J.C., Richez, C., 1985. Water masses and circulation in the Western Alboran Sea and in the Straits of Gibraltar. Prog. Oceanogr. 15, 157–216. https://doi.org/10.1016/0079-6611(85)90031-X.
Gaspar-Escribano, J.M., Rivas-Medina, A., Parra, H., Cabañas, L., Benito, B., Ruiz Barajas, S., Martínez Solares, J.M., 2015. Uncertainty assessment for the seismic hazard map of Spain. Eng. Geol. 199, 62–73. https://doi.org/10.1016/j.enggeo.2015.10.001.
Gatter, R., Clare, M.A., Hunt, J.E., Watts, M., Madhusudhan, B.N., Talling, P.J., Huhn, K., 2020. A multi-disciplinary investigation of the AFEN Slide: the relationship between contourites and submarine landslides. In: Georgiopoulou, A., Amy, L.A., Benetti, S., Chaytor, J.D., Clare, M.A., Gamboa, D., Mountjoy, J.J. (Eds.), Subaqueous Mass Movements and their Consequences: Advances in Process Understanding, Monitoring and Hazard Assessments, 500. Geological Society, London, Special Publications, pp. 173–193. https://doi.org/10.1144/SP500-2019-184.
Hernández-Molina, F.J., Llave, E., Somoza, L., Fernández-Puga, M.C., Maestro, A., León, R., Barnolas, A., Medialdea, T., García, M., Vázquez, J.T., Díaz del Río, V., Fernández-Salas, L.M., Lobo, F., Alveirinho Dias, J.M., Rodero, J., Gardner, J., 2003. Looking for clues to paleoceanographic imprints: a diagnosis of the Gulf of Cádiz contourite depositional systems. Geology 31, 19–22.
Hernández-Molina, F.J., Serra, N., Stow, D.A.V., Llave, E., Ercilla, G., Van Rooij, D., 2011. Along-slope oceanographic processes and sedimentary products around the Iberian margin. Geomar. Lett. 31, 315–341. https://doi.org/10.1007/s00367-011-0242-2.
Ikari, M.J., Kopf, A.J., 2015. The role of cohesion and overconsolidation in submarine slope failure. Mar. Geol. 369, 153–161. https://doi.org/10.1016/j.margeo.2015.08.012.
Jacobsen, J.P., Thomsen, H., 1934. Periodical variations in temperature and salinity in the Strait of Gibraltar. In: James Johnstone Memorial. University Press, pp. 275–293.
Juan, C., Ercilla, G., Hernández-Molina, F.J., Estrada, F., Alonso, B., Casas, D., García, M., Farran, M.L., Llave, E., Palomino, D., Vázquez, J.-T., Medialdea, T., Gorini, C., D'Acremont, E., El Moumni, B., Ammar, A., 2016. Seismic evidence of current-controlled sedimentation in the Alboran Sea during the Pliocene and Quaternary: palaeoceanographic implications. Mar. Geol. 378, 292–311. https://doi.org/10.1016/j.margeo.2016.01.00.
Juan, C., Ercilla, G., Estrada, F., Alonso, B., Casas, D., Vázquez, J.T., d'Acremontd, E., Medialdea, T., Hernández-Molina, F.J., Gorini, C., El Moumni, B., Valencia, J., 2020. Multiple factors controlling the deep marine sedimentation of the Alboran Sea (SW Mediterranean) after the Zanclean Atlantic Mega-flood. Mar. Geol. 423, 106138.
Krastel, S., Lehr, J., Winkelmann, D., Schwenk, T., Preu, B., Strasser, M., Wynn, R.B., Georgiopoulou, A., Hanebuth, T.J.J., 2014. Mass wasting along Atlantic Continental margins: a comparison between NW-Africa and the de la Plata River Region (Northern Argentina and Uruguay). In: Krastel, S., et al. (Eds.), Submarine Mass Movements and Their Consequences. Advances in Natural and Technological Hazards Research, 37. Springer, Cham. https://doi.org/10.1007/978-3-319-00972-8_41.
La Violette, P.E., Kinder, T.H., Green, D.W., 1986. Measurement of internal waves in the Strait of Gibraltar using a shore-based radar. In: Technical Report 118, Naval Ocean Research and Development Activity, National Space Technology Laboratory, Bay of St. Louis, Miss, p. 13.
Laberg, J.S., Camerlenghi, A., 2008. The significance of contourites for submarine slope stability. In: Rebesco, M., Camerlenghi, A. (Eds.), Contourites. Developments in Sedimentology, 60. Elsevier, pp. 537–556. https://doi.org/10.1016/S0070-4571(08)10025-5.
Laberg, J.S., Baeten, N.J., Vanneste, M., Forsberg, C.F., Forwick, M., Haflidason, H., 2016. Sediment failure affecting muddy contourites on the continental slope offshore northern Norway: lessons learned and some outstanding issues. In: Lamarche, G., et al. (Eds.), Submarine Mass Movements and their Consequences. Advances in Natural and Technological Hazards Research, 41. Springer, Cham. https://doi.org/10.1007/978-3-319-20979-1_28.
Lee, H.J., Baraza, J., 1999. Geotechnical characteristics and slope stability in the Gulf of Cadiz. Mar. Geol. 155, 173–190.
Lee, H.J., Locat, J., Desgagnes, P., Parsons, J.D., McAdoo, B.G., Orange, D.L., Puig, P., Wong, F.L., Dartnell, P., Boulanger, E., 2007. Submarine mass movements on continental margins. In: Continental Margin Sedimentation, edited by C. A. Nittrouer, ch5, Blackwell, U. K, pp. 213–274. https://doi.org/10.1002/9781444304398.
Leynaud, D., Mienert, J., Nadim, F., 2004. Slope stability assessment of the Helland Hansen area offshore the mid-Norwegian margin. Mar. Geol. 213, 457–480.
Lobo, F.J., Ercilla, G., Fernández-Salas, L.M., Gámez, D., 2014. The Iberian Mediterranean shelves. Geol. Soc. Mem. 41 (1), 147–170.
Locat, J., Lee, H.J., 2002. Submarine landslides: advances and challenges. Can. Geotech. J. 39, 193–212. https://doi.org/10.1139/t01-089.
López-González, N., Alonso, B., Juan, C., Ercilla, G., Bozzano, G., Cacho, I., Casas, D., Palomino, D., Vázquez, J.T., Estrada, F., Bárcenas, P., d'Acremont, E., Gorini, C., El Moumni, B., 2019. 133,000 years of sedimentary record in a contourite drift in the Western Alboran Sea: sediment sources and paleocurrent reconstruction. Geosciences 9, 345. https://doi.org/10.3390/geosciences9080345.
Low, H.E., Lunne, T., Andersen, K.H., Sjursen, M.A., Li, X., Randolph, M.F., 2010. Estimation of intact and remoulded undrained shear strengths from penetration tests in soft clays. Géotechnique 66 (11), 843–859. https://doi.org/10.1680/geot.9.P.017.
Lüdmann, T., Wiggershaus, S., Betzler, C., Hübscher, C., 2012. Southwest Mallorca Island: a cool-water carbonate margin dominated by drift deposition associated with giant mass wasting. Mar. Geol. 307, 73–87. https://doi.org/10.1016/j.margeo.2011.09.008.
Lunne, T., 2012. The CPT in offshore soil investigations - a historic perspective. Geomech. Geoeng. Intern. J. 1, 1–27.

Maldonado, A., Campillo, A.C., Mauffret, A., Alonso, B., Woodside, J., Campos, J., 1992. Alboran Sea late Cenozoic tectonic and stratigraphic evolution. Geomar. Lett. 12, 179–186. https://doi.org/10.1007/BF02084930.

Martínez-García, P., Comas, M., Lonergan, L., Watts, A.B., 2017. From extension to shortening: Tectonic inversion distributed in time and space in the Alboran Sea, western Mediterranean. Tectonics 36, 2777–2805.

Martorelli, E., Bosman, A., Casalbore, D., Falcini, F., 2016. Interaction of down-slope and along-slope processes off Capo Vaticano (southern Tyrrhenian Sea, Italy), with particular reference to contourite-related landslides. Mar. Geol. 378, 43–55.

Mayne, P.W., 2010. Soil parameter evaluation from hybrid in-situ penetration-geophysics testing. Geotechn. Spec. Public. 199, 1049–1058.

McAdoo, B.G., Watts, P., 2004. Tsunami hazard from submarine landslides on the Oregon continental slope. Mar. Geol. 203, 235–245. https://doi.org/10.1016/S00253227(03)00307-4.

McAdoo, B.G., Capone, M.K., Minder, J., 2004. Seafloor geomorphology of convergent margins: implications for Cascadia seismic hazard. Tectonics 23. https://doi.org/10.1029/2003TC001570. TC6008.

McCave, I.N., Hall, I.R., Antia, A.N., Chou, L., Dehairs, F., Lampitt, R.S., Thomsen, L., van Weering, T.C.E., Wollast, R., 2001. Distribution, composition and flux of particulate material over the European margin at 47°–50°N. Deep-Sea Res. II Top. Stud. Oceanogr. 48 (14–15), 3107–3139. https://doi.org/10.1016/S0967-0645(01)00034-0.

Mestdagh, T., Lobo, F.J., Llave, E., Hernández-Molina, J., García-Ledesma, A., Puga-Bernabéu, A., Fernández-Salas, L.-M., Rooij, D.V., 2020. Late Quaternary multi-genetic processes and products on the northern Gulf of Cadiz upper continental slope (SW Iberian Peninsula). Mar. Geol. 427, 106214.

Miramontes, E., Garziglia, S., Sultan, N., Jouet, G., Cattaneo, A., 2018. Morphological control of slope instability in contourites: a geotechnical approach. Landslides 15, 1085–1095. https://doi.org/10.1007/s10346-018-0956-6.

Mulder, T., Voisset, M., Lecroart, P., Le Drezen, E., Gonthier, E., Hanquiez, V., Faugères, J.C., Habgood, E., Hernández-Molina, F.J., Estrada, F., Llave, E., Poirier, D., Gorini, C., Fuchey, Y., Voelker, A., Freitas, P., Lobo-Sánchez, F., Fernández, L.M., Kenyon, N.H., Morel, J., 2003. The Gulf of Cadiz: an unstable giant contouritic levee. Geo-Mar. Lett. 23, 7–18.

Müller-Vonmoos, M., Loken, T., 1989. The searing behavior of clays. Appl. Clay Sci. 4, 125–141.

NCSE-02, 2009. Norma de construcción sismorresistente. Ministerio de Fomento, España.

Palomino, D., Vázquez, J.T., Ercilla, G., Alonso, B., López-González, N., Díaz-del-Río, V., 2011. Interaction between seabed morphology and water masses around the seamounts on the Motril marginal Plateau (Alboran Sea, Western Mediterranean). Geo-Mar. Lett. 31, 465–479.

Platt, J.P., Vissers, R.L.M., 1989. Extensional collapse of thickened continental lithosphere: a working hypothesis for the Alboran Sea and Gibraltar arc. Geology 17, 540–543.

Puig, P., Palanques, A., Guillén, J., El Khatab, M., 2004. Role of Internal Waves in the Generation of Nepheloid Layers on the Northwestern Alboran Slope: Implications for Continental Margin Shaping.

Puzrin, A.M., Gray, T., Hill, A.J., 2015. Significance of the actual non-linear slope geometry for catastrophic failure in submarine landslides. Proc. R. Soc. A. Math. Phys. Eng. Sci. 471 (2175): 1–25. J. Geophys. Res. 109, C09011 https://doi.org/10.1029/2004JC002394.

Rebesco, M., Hernández-Molina, F.J., Van Rooij, D., Wåhlin, A., 2014. Contourites and associated sediments controlled by deep-water circulation processes: state-of-the-art and future considerations. Mar. Geol. 352, 111–154. https://doi.org/10.1016/j.margeo.2014.03.011.

Robertson, P.K., 1990. Soil classification using the cone penetration test. Can. Geotech. J. 27, 151–158.

Robertson, P.K., Cabal, K.L., 2014. Guide to Cone Penetration Testing for Geotechnical Engineering, 6th ed. Gregg Drilling & Testing, Inc.

Roesner, A., Wiemer, G., Kreiter, S., Wenau, S., Wu, T.W., Courboulex, F., Kopf, A., 2019. Impact of seismicity on Nice slope stability—Ligurian Basin, SE France: a geotechnical revisit. Landslides 16 (1), 23–35. https://doi.org/10.1007/s10346-018-1060-7.

Sawyer, D.E., DeVore, J.R., 2015. Elevated shear strength of sediments on active margins: evidence for seismic strengthening. Geophys. Res. Lett. 42 (23), 10216–10221. https://doi.org/10.1002/2015GL066603.

Steiner, A., Kopf, A.J., Henry, P., Stegmanna, S., Apprioual, R., Pelleauc, P., 2015. Cone penetration testing to assess slope stability in the 1979 Nice landslide area (Ligurian margin, SE France). Mar. Geol. 369, 162–181.

Stow, D.A.V., Faugères, J.C., 2008. Contourite facies and the facies model. In: Rebesco, M., Camerlenghi, A. (Eds.), Contourites Developments in Sedimentology, 60. Elsevier, pp. 223–256.

Stow, D.A.V., Faugères, J.C., Gonthier, E., Cremer, M., Llave, E., Hernández-Molina, F.J., Somoza, L., Díaz del Río, V., 2002. Faro-albufeira drift complex, Northern Gulf of Cádiz. In: Stow, D.A.V., Pudsey, C.J., Howe, J.A., Faugères, J.-C., Viana, A.R. (Eds.), Deep-Water Contourite Systems: Modern Drifts and Ancient Series, Seismic and Sedimentary Characteristics, 22. Geol. Soc. Lond. Mem., pp. 137–154 (1).

Strasser, M., Stegmann, S., Bussmann, F., Anselmetti, F.S., Rick, B., Kopf, A., 2007. Quantifying subaqueous slope stability during seismic shaking: Lake Lucerne as model for ocean margins. Mar. Geol. 240, 77–97.

Strasser, M., Henry, P., Kanamatsu, T., Thu, M.K., Moore, G.F., Scientists, I.E., 2012. Scientific drilling of mass-transport deposits in the Nankai accretionary wedge: First results from IODP expedition 333. In: Yamada, Y., Kawamura, K., Ikehara, K., Ogawa, Y., Urgeles, R., Mosher, D., Chaytor, J., Strasser, M. (Eds.), Submarine Mass Movements and their Consequences. Advances in Natural and Technological Hazards Research. Springer, Dordrecht, NL, pp. 671–681.

Strozyk, F., Strasser, M., Förster, A., Kopf, A., Huhn, K., 2010. Slope failure repetition in active margin environments: constraints from submarine landslides in the Hellenic fore arc, eastern Mediterranean. J. Geophys. Res. Solid Earth 115. https://doi.org/10.1029/2009JB006841.B08103.

Teixeira, M., Terrinha, P., Roque, C., Rosa, M., Ercilla, G., Casas, D., 2019. Interaction of along-slope and downslope processes in the Alentejo margin (SW Iberia) - implications on slope stability. Mar. Geol. 410, 88–108.

Thian, S.Y., Lee, C.Y., 2017. Cyclic stress-controlled tests on offshore clay. J. Rock Mech. Geotech. Eng. 9, 376–381. https://doi.org/10.1016/j.jrmge.2016.06.013.

Vázquez, A., 2006. Ondas Internas en el Estrecho de Gibraltar y Procesos de Mezcla Inducidos. Thesis. Universidad de Cádiz, In Spanish, p. 292. Available online in. https://www.google.com/search?q=v%C3%A1zquez%2C+2006%2C+solitones&oq=v%C3%A1zquez%2C+2006%2C+solitones&aqs=chrome.69i57.8852j0j1&sourceid=chrome&ie=UTF-8.

Yenes, M., Casas, D., Nespereira, J., Monterrubio, S., Ercilla, G., López-González, N., 2019. Galicia Bank sediment transport activity in response to continuous sedimentary instability dynamics: a geotechnical perspective. Int. J. Earth Sci. 108, 2545–2560. https://doi.org/10.1007/s00531-019-01776-w.

Yenes, M., Monterrubio, S., Nespereira, J., Casas, D., 2020. Apparent overconsolidation and its implications for submarine landslides. Eng. Geol. 264, 105375. https://doi.org/10.1016/j.enggeo.2019.105375.